ChemComm

Check for updates

Bulk ionic screening lengths from extremely large-scale molecular dynamics simulations†

Johannes Zeman, [ID] [a] Svyatoslav Kondrat [ID] [bcd] and Christian Holm [ID] *[a]

Recent experiments have reported anomalously large screening lengths of interactions between charged surfaces confining concentrated electrolytes and ionic liquids. Termed underscreening, this effect was ascribed to bulk properties of dense ionic systems. Herein, we study bulk ionic screening with extremely large-scale molecular dynamics simulations, allowing us to assess the range of distances relevant to the experiments. Our results yield two screening lengths satisfying distinct scaling relations. However, with an accuracy of 10^{-5} $k_B T$ in interionic potentials of mean force, we find no signs of underscreening, suggesting that other than bulk effects might be at play in the experiments.

Concentrated electrolytes and room-temperature ionic liquids (ILs) are playing an increasingly important role in science and technology, with applications ranging from organic synthesis, catalysis and analytical chemistry to electrochemical energy storage.[1–4] Tailoring their properties requires a fundamental understanding of the intra- and intermolecular mechanisms governing their internal structure and dynamics. A puzzling observation, attributed to the bulk properties of concentrated electrolytes and ionic liquids, is the so-called underscreening, which is an anomalously large decay length of electrostatic interactions mediated by these liquids, as reported by recent surface force balance (SFB) experiments.[5–9]

For dilute electrolytes, the decay length is well described by the Debye–Hückel theory[10] with the Debye screening length $\lambda_D^2 = \dfrac{\varepsilon_0 \varepsilon_r k_B T}{\sum_i \rho_i z_i^2 e^2}$, where ε_0 is the vacuum permittivity, ε_r the

[a] *Institute for Computational Physics, University of Stuttgart, D-70569 Stuttgart, Germany. E-mail: holm@icp.uni-stuttgart.de*

[b] *Department of Complex Systems, Institute of Physical Chemistry, Polish Academy of Sciences, 01-224 Warsaw, Poland*

[c] *Max-Planck-Institut für Intelligente Systeme, Heisenbergstraße 3, 70569 Stuttgart, Germany*

[d] *IV. Institut für Theoretische Physik, Universität Stuttgart, Pfaffenwaldring 57, 70569 Stuttgart, Germany*

† Electronic supplementary information (ESI) available. See DOI: 10.1039/d0cc05023g

relative dielectric permittivity of a homogeneous background medium, k_B the Boltzmann constant, T the absolute temperature, ρ_i and z_i the number density and the valency of species i, and e the elementary charge. In the high-concentration regime, classical liquid state theories predict a damped oscillatory behavior, which is either core- or electrostatics-dominated, with the screening length exceeding λ_D and growing with increasing electrolyte concentration.[11–14] The aforementioned SFB experiments reported the emergence of a screening length λ_S roughly an order of magnitude larger than the ones predicted by classical theories.[5–9] In these experiments, the force was measured between two atomically flat, charged surfaces, confining neat ILs or electrolytes, and λ_S was extracted by fitting the force to a monotonic, exponentially decaying function of surface separation. All analyzed experimental data for λ_S *versus* ion concentration collapsed onto a single curve if appropriately rescaled. The corresponding scaling relation[15,16]

$$\frac{\lambda_S}{\lambda_D} \propto \left(\frac{d}{\lambda_D} \right)^\alpha, \tag{1}$$

where d is the ion diameter and the scaling exponent $\alpha = 3$, has been suggested to be a bulk property of concentrated electrolytes.[15] This behavior challenges our understanding of bulk ionic systems.

Herein, we report on long-range screening in selected bulk ionic systems obtained by extremely large-scale molecular dynamics (MD) simulations in volumes that encompass several of the experimentally measured screening lengths. As an example of a neat IL, we investigate 1-butyl-3-methylimidazolium hexafluorophosphate ($[C_4C_1Im]^+[PF_6]^-$) as there exist well-tested MD force fields for both all-atom and coarse-grained representations of this IL. We also perform all-atom simulations of aqueous sodium chloride (NaCl) solutions with concentrations ranging from 1 to 5.2 mol l^{-1}. Finally, we conduct a series of simulations of 1-butyl-3-methylimidazolium bis(trifluoromethylsulfonyl)imide ($[C_4C_1Im]^+[NTF_2]^-$) in a racemic propylene carbonate (PC) mixture (equal amounts of (R)- and (S)-propylene carbonate) for IL mole fractions between $x = 0.05$ and $x = 1$ (pure $[C_4C_1Im]^+[NTF_2]^-$). This

system is similar to the solution of 1-butyl-1-methylpyrrolidinium bis(trifluoromethylsulfonyl)imide ($[C_4C_1Pyrr]^+[NTF_2]^-$) in PC studied in ref. 9. All system compositions are listed in Section S1 of the ESI.†

Simulations have been performed with the GROMACS 2016.3 simulation package[17] in the NpT ensemble using cubic boxes under periodic boundary conditions at temperature T = 300 K and pressure p = 1 bar (simulation parameters are listed in Section S3 of the ESI†). For ILs, we employed the 0.8*OPLS-2009IL all-atom force field of Doherty et $al.$[18] and the ILM2 force field of Roy and Maroncelli[19] for the coarse-grained description of $[C_4C_1Im]^+[PF_6]^-$. To simulate aqueous NaCl solutions, we used the KBFF ion parameters of Weerasinghe and Smith[20] in conjunction with the extended simple point charge (SPC/E) water model.[21] To describe the PC interactions for the simulations of $[C_4C_1Im]^+[NTF_2]^-$ in PC, we used the parameters provided by Takeuchi et $al.$[22]

From the simulation trajectories, we computed radial distribution functions (RDFs) $g_{XY}(r)$ (X and Y denote ionic species). For our large-scale ionic systems, the computation of RDFs with GROMACS analysis tools would have taken several years to complete. We have therefore developed our own optimized analysis tool based on MDAnalysis[23,24] and MPI for Python,[25–27] allowing the evaluation of RDFs on hundreds of CPUs in parallel.[28]

In spatially homogeneous systems, the effective interaction between ions X and Y is described by the potential of mean force (PMF), which is related to the RDF by $w_{XY}(r) = -k_B T \ln(g_{XY}(r))$. If the observed long-range decay[5–9] is a property of bulk ionic liquids, one can expect the same asymptotic decay in an effective ion–ion interaction potential,[29] and hence, in the corresponding PMF. Our further discussion will therefore be based on the analysis of PMFs.

Before discussing our results, it is important to stress that the experimentally observed transition between the damped oscillatory and the 'under-screened' monotonic regime occurred at separations between 4 and 7 nm for ILs, and up to 3 nm for NaCl.[9,30] Thus, simulated systems have to be sufficiently large to allow the evaluation of PMFs far beyond these separations. Furthermore, ILs exhibit slow structural relaxations, necessitating simulation times of several hundred nanoseconds.[31] Unlike previous work,[32] our simulations strictly fulfill both requirements (see Section S2.3 of the ESI† for a comparison of PMFs for different simulation times). Since the magnitude of underscreening is expected to be small, possibly interfering with statistical errors, we also performed rigorous error analyses for all data series, taking temporal correlations into account.[28]

For distances up to $r \approx 8.5$ nm, the PMF is well-described by an exponentially damped oscillatory hyperbolic decay

$$\lim_{r \to \infty} w_{XY}(r) \propto \frac{A}{r} \cos(k(r - \phi)) \exp\left(-\frac{r}{\lambda_S}\right), \qquad (2)$$

where A and ϕ are the amplitude and the phase shift, λ_S is the PMF's asymptotic decay length, and the wave vector k determines the wavelength of its oscillation. The envelope of this decay is indicated in Fig. 1a by a dashed orange line (we
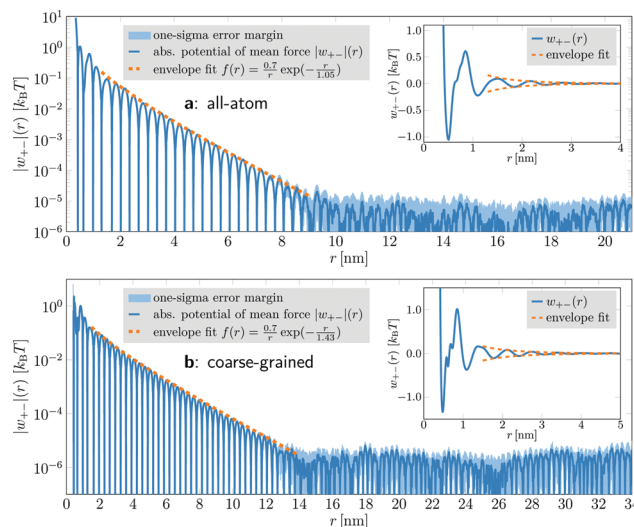

Fig. 1 Absolute value of the PMF $|w_{+-}|(r)$ between anions and cations (blue lines) in $[C_4C_1Im]^+[PF_6]^-$. (a) All-atom model. $w_{+-}(r)$ follows an oscillatory decay up to $r \approx 8.5$ nm, with the decay envelope (dashed, orange line) described by $f(r) = a/r \exp(-r/\lambda_S)$ with a = 0.7 $k_B T$ and λ_S = 1.05 nm. For $r > 8.5$ nm, the potential enters a region of almost constant noise level with rather high uncertainty (light blue area). Inset: The same anion–cation PMF $w_{+-}(r)$ with linear y-axis scaling. (b) Coarse-grained model. The qualitative features are the same as in the all-atom model, but the covered distances are up to 34 nm. The extracted screening length λ_S = 1.43 nm is larger than in the all-atom simulations due to its coarse-grained description.

excluded the region $r < 1.3$ nm from the analysis because it is strongly affected by short-ranged Lennard-Jones interactions). The extracted decay length λ_S = 1.05 nm is consistent with classical theories.[11–14] The cation–cation and anion–anion PMFs exhibit a similar behavior with the same decay length.[28] The statistical uncertainty is quite high for $r \gtrsim 8.5$ nm and a hypothetical monotonic decay in this region might be hidden in the noise. However, experiments with similar ILs[9] suggest an onset of the monotonic decay already at smaller separations, which is not present in our data.

In coarse-grained simulations of $[C_4C_1Im]^+[PF_6]^-$, the box edge length was almost 50 nm and the system comprised 358 296 ion pairs (1 433 184 interaction sites). The PMFs were calculated for distances up to 34 nm (Fig. 1b). They exhibit the same qualitative behavior as the all-atom model, but yield a larger decay length λ_S = 1.43 nm, which can be attributed to the coarse-grained description. Due to the larger number of ions in the system, the increased statistical accuracy allowed us to resolve the oscillatory decay at distances up to 13 nm. For larger distances, the PMF again enters a region of almost constant noise level.

Next, we analyze a 4.43 mol l^{-1} aqueous NaCl solution. This system comprised 216 000 ion pairs and 2 458 296 water molecules (7 806 888 atoms in total) in a simulation box with an edge length of 43.25 nm. The cation–anion PMF obtained from a 200 ns simulation run is displayed in Fig. 2. Although in this case a superposition of several damped oscillatory functions was needed to fit the PMFs ($cf.$ eqn (3)), up to 2.2 nm their envelope could still be approximated by a single decay (dashed
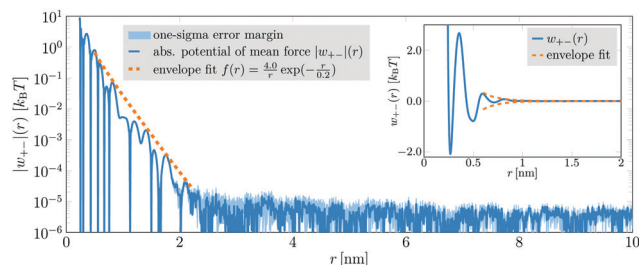
Fig. 2 Absolute value of the PMF $|w_{+-}|(r)$ between anions and cations (blue line) in a 4.43 mol l^{-1} aqueous NaCl solution. Up to a distance of about 2.2 nm, $w_{+-}(r)$ exhibits an oscillatory decay which is comprised of a superposition of several oscillations with different parameters. Nevertheless, the envelope of the decay (dashed, orange line) can be approximated by $f(r) = a/r \exp(-r/\lambda_S)$ with amplitude $a = 4.0 \, k_BT$ and decay length $\lambda_S = 0.2$ nm. For distances larger than 2.2 nm, the potential lies in the order of the uncertainty level of about $10^{-5} \, k_BT$. Its further decay is not a feature of the system but simply due to the statistical error, which decreases with increasing distance.

orange line in Fig. 2). The extracted decay length $\lambda_S = 0.2$ nm is again consistent with classical theories.[11–14] For distances exceeding 2.2 nm, the PMF becomes very noisy and no distinct oscillations are discernible. In this region, the PMF's envelope may seem to follow a long-ranged decay. However, this decay is entirely due to statistical noise, which decreases with distance. It can be shown that the noise in the PMF of an ideal gas, comprising the same number of particles in the same volume, exhibits the very same decay.[28] Hence, in this case, there is also no anomalously long-ranged monotonic decay of interionic interactions detectable within an accuracy of $\approx 10^{-5} \, k_BT$.

To study the concentration dependence of the screening lengths, we simulated aqueous NaCl electrolytes for ion concentrations ranging from 1.16 to 5.19 mol l^{-1}. Each system comprised 3750 ion pairs and a concentration-dependent number of water molecules. In addition, we conducted all-atom simulations of [C$_4$C$_1$Im]$^+$[NTf$_2$]$^-$ in PC at various concentrations. As there has been no sign of anomalously large screening lengths, we chose to use smaller simulation boxes in favor of covering a larger number of IL concentrations. With the exception of the two lowest concentrations, all systems contained 500 ion pairs and a suitably adjusted number of PC molecules. For each system, we performed up to four independent simulation runs with more than 1 µs per run.

Unlike for neat [C$_4$C$_1$Im]$^+$[PF$_6$]$^-$, these systems required a superposition of several oscillatory exponentially damped hyperbolas

$$f(r) = \sum_{n=1}^{k} \frac{A_n}{r} \cos(\omega_n r - \phi_n) \exp\left(-\frac{r}{\lambda_n}\right) \tag{3}$$

to fit the data. We found that $k = 2$ was sufficient to obtain an excellent fit for all IL mixtures in the range $1.2 \leq r \leq 3$ nm. The PMFs of aqueous NaCl solutions required $k = 3$ to fit in the range $0.8 \leq r \leq 2$ nm (for fit parameters see Sections S2.4 and S2.5 of the ESI† and Fig. S13 of the ESI† for fitting with $k = 2$). Fig. 3 shows that the obtained screening lengths $\lambda_S = \max(\lambda_n)$
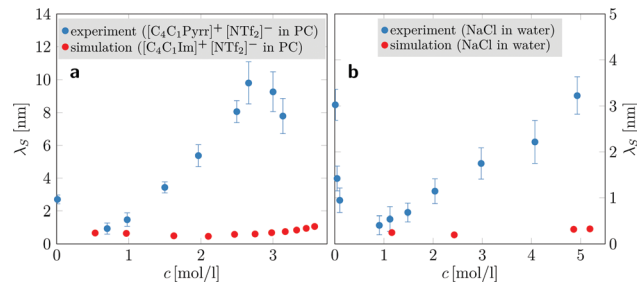
are almost an order of magnitude smaller than those measured in SFB experiments of similar systems.[9]

Determining scaling relations for the correlation lengths, akin to eqn (1), requires the knowledge of an average ion diameter d and the Debye length λ_D. For [C$_4$C$_1$Im]$^+$[NTf$_2$]$^-$, we used the number of ion pairs N_{IP} and the simulation box volume V to determine $d = \frac{1}{2}(V/N_{IP})^{\frac{1}{3}} \approx 0.39$ nm; for NaCl we took $d = 0.294$ nm from ref. 9. Calculating λ_D requires the knowledge of the static relative dielectric permittivity ε_r of a background medium. We computed ε_r of the entire system, as in ref. 15, by using the Einstein–Helfand method.[33] The obtained values of ε_r compare well with the available experimental data for pure PC[34] and pure [C$_4$C$_1$Im]$^+$[PF$_6$]$^-$.[35] For aqueous NaCl, our ε_r is systematically lower than the experimental values, due to the SPC/E model underestimating the permittivity of water.[36] Nevertheless, the concentration-dependent trend is well reproduced (cf. ref. 37). The values of ε_r are listed in Section S2.2 of the ESI.†

Fig. 4 shows the ratio λ_n/λ_D ($n = 1, 2$) as a function of d/λ_D with λ_n obtained from fitting the PMFs to eqn (3). The asymptotic linear and quadratic scaling

$$\frac{\lambda_n}{\lambda_D} \propto \left(\frac{d}{\lambda_D}\right)^n \tag{4}$$

is clearly visible in Fig. 4. Interestingly, the two screening lengths cross each other, so that the screening length with the quadratic scaling prevails at high concentrations.[38] For NaCl, the screening length λ_3 is smaller than λ_1 and λ_2, but the values are too scattered to deduce any scaling (Fig. S12 of the ESI†). Recently, Coles et al.[32] have reported on MD simulations of [Li]$^+$[TFSI]$^-$ and extracted the exponent $\alpha \approx 1.3$ (eqn (1)). However, this exponent is probably because they fitted the radial distribution functions with only one exponentially damped oscillatory decay (eqn (2)).

In conclusion, our extremely large-scale MD simulations of concentrated electrolytes and neat ionic liquids allowed us to calculate interionic PMFs with unprecedented precision and to analyze their behavior in a range of distances relevant to experiments.[5–9] We revealed the existence of two screening

Fig. 3 Concentration-dependent screening lengths λ_S obtained from MD simulations compared to those obtained from experimental SFB measurements for similar ionic species. (a) Experimentally determined electrostatic screening lengths of [C$_4$C$_1$Pyrr]$^+$[NTf$_2$]$^-$ in PC (blue dots) compared to simulation results of [C$_4$C$_1$Im]$^+$[NTf$_6$]$^-$ in PC (red dots). (b) Screening lengths of aqueous NaCl solutions (experiment: blue dots; simulation: red dots). Experimental data are taken from ref. 9.
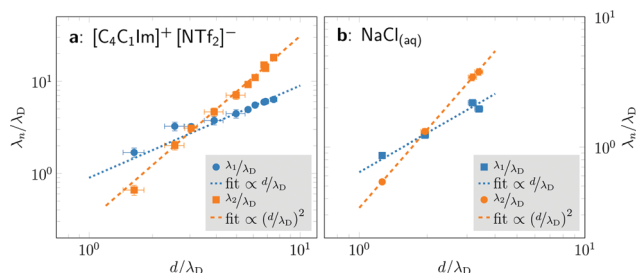
Fig. 4 Scaling of the concentration-dependent screening lengths of $[C_4C_1Im]^+[NTf_2]^-$ in propylene carbonate (left) and NaCl in water (right) as determined by fits of eqn (3) to cation–anion PMFs $w_{+-}(r)$. The ratio of the screening λ_n to the concentration-dependent Debye length λ_D is shown as a function of the average ion diameter d divided by λ_D. For both substances, we see two decay lengths, each corresponding to a distinct wavelength $2\pi/\omega_n$, and both exhibiting a power law dependence. For both systems, the asymptotic decay length ratio for high concentrations λ_2/λ_D is proportional to $(d/\lambda_D)^2$.

lengths showing linear and quadratic scaling, eqn (4). However, within a PMF accuracy of $10^{-5}\ k_BT$, we observed no evidence for an anomalously long-ranged, monotonic decay in effective ionic interactions. These results demonstrate that underscreening is unlikely an equilibrium bulk property of concentrated ionic systems.

We finish by noting that, so far, there is no theory of bulk ionic systems consistent with underscreening and cubic scaling (eqn (1) with $\alpha = 3$).[38–41] Interestingly, most recent SFB results, while showing extremely large decay lengths, have demonstrated inconsistencies with the cubic scaling for $[EMIM]^+[EtSO_4]^-$.[42,43] Furthermore, to our knowledge, only one atomic force microscopy (AFM) study[44] reported underscreening, and only at elevated temperatures, while other AFM measurements have not.[6] Thus, a careful examination of underscreening, preferentially by complementary experimental techniques appears necessary, while other than bulk ionic effects may need to be considered to explain the SFB results of ref. 5–9.

Conflicts of interest

There are no conflicts to declare.

References

1 R. D. Rogers and K. R. Seddon, *Science*, 2003, **302**, 792–793.
2 S. Pandey, *Anal. Chim. Acta*, 2006, **556**, 38–45.
3 R. Hayes, G. G. Warr and R. Atkin, *Chem. Rev.*, 2015, **115**, 6357–6426.
4 Z. Lei, B. Chen, Y.-M. Koo and D. R. MacFarlane, *Chem. Rev.*, 2017, **117**, 6633–6635.
5 M. A. Gebbie, M. Valtiner, X. Banquy, E. T. Fox, W. A. Henderson and J. N. Israelachvili, *Proc. Natl. Acad. Sci. U. S. A.*, 2013, **110**, 9674–9679.
6 T. Baimpos, B. R. Shrestha, S. Raman and M. Valtiner, *Langmuir*, 2014, **30**, 4322–4332.
7 R. M. Espinosa-Marzal, A. Arcifa, A. Rossi and N. D. Spencer, *J. Phys. Chem. Lett.*, 2014, **5**, 179–184.
8 M. A. Gebbie, H. A. Dobbs, M. Valtiner and J. N. Israelachvili, *Proc. Natl. Acad. Sci. U. S. A.*, 2015, **112**, 7432–7437.
9 A. M. Smith, A. A. Lee and S. Perkin, *J. Phys. Chem. Lett.*, 2016, **7**, 2157–2163.
10 P. Debye and E. Hückel, *Phys. Z*, 1923, **24**, 185–206.
11 P. Attard, *Phys. Rev. E: Stat., Nonlinear, Soft Matter Phys.*, 1993, **48**, 3604–3621.
12 R. Evans, R. J. F. Leote de Carvalho, J. R. Henderson and D. C. Hoyle, *J. Chem. Phys.*, 1994, **100**, 591–603.
13 R. J. F. Leote de Carvalho and R. Evans, *Mol. Phys.*, 1994, **83**, 619–654.
14 L. M. Varela, M. García and V. Mosquera, *Phys. Rep.*, 2003, **382**, 1–111.
15 A. A. Lee, C. S. Perez-Martinez, A. M. Smith and S. Perkin, *Phys. Rev. Lett.*, 2017, **119**, 026002.
16 A. A. Lee, C. S. Perez-Martinez, A. M. Smith and S. Perkin, *Faraday Discuss.*, 2017, **199**, 239–259.
17 M. J. Abraham, T. Murtola, R. Schulz, S. Páll, J. C. Smith, B. Hess and E. Lindahl, *SoftwareX*, 2015, **1**, 19–25.
18 B. Doherty, X. Zhong, S. Gathiaka, B. Li and O. Acevedo, *J. Chem. Theory Comput.*, 2017, **13**, 6131–6145.
19 D. Roy and M. Maroncelli, *J. Phys. Chem. B*, 2010, **114**, 12629–12631.
20 S. Weerasinghe and P. E. Smith, *J. Chem. Phys.*, 2003, **119**, 11342–11349.
21 H. J. C. Berendsen, J. R. Grigera and T. P. Straatsma, *J. Phys. Chem.*, 1987, **91**, 6269–6271.
22 M. Takeuchi, Y. Kameda, Y. Umebayashi, S. Ogawa, T. Sonoda, S.-i. Ishiguro, M. Fujita and M. Sano, *J. Mol. Liq.*, 2009, **148**, 99–108.
23 N. Michaud-Agrawal, E. J. Denning, T. B. Woolf and O. Beckstein, *J. Comput. Chem.*, 2011, **32**, 2319–2327.
24 R. J. Gowers, M. Linke, J. Barnoud, T. J. E. Reddy, M. N. Melo, S. L. Seyler, J. Domański, D. L. Dotson, S. Buchoux, I. M. Kenney and O. Beckstein, Proceedings of the 15th Python in Science Conference, 2016, pp. 98–105.
25 L. D. Dalcín, R. R. Paz and M. Storti, *J. Parallel Distrib. Comput.*, 2005, **65**, 1108–1115.
26 L. D. Dalcín, R. R. Paz, M. Storti and J. D'Elía, *J. Parallel Distrib. Comput.*, 2008, **68**, 655–662.
27 L. D. Dalcín, R. R. Paz, P. A. Kler and A. Cosimo, *Adv. Water Resour.*, 2011, **34**, 1124–1139.
28 J. Zeman, S. Kondrat and C. Holm, to be published.
29 R. Kjellander, *J. Chem. Phys.*, 2018, **148**, 193701.
30 M. A. Gebbie, A. M. Smith, H. A. Dobbs, A. A. Lee, G. G. Warr, X. Banquy, M. Valtiner, M. W. Rutland, J. N. Israelachvili, S. Perkin and R. Atkin, *Chem. Commun.*, 2017, **53**, 1214–1224.
31 S. Gabl, C. Schröder and O. Steinhauser, *J. Chem. Phys.*, 2012, **137**, 094501.
32 S. W. Coles, C. Park, R. Nikam, M. Kanduč, J. Dzubiella and B. Rotenberg, *J. Phys. Chem. B*, 2020, **124**, 1778–1786.
33 C. Schröder, M. Haberler and O. Steinhauser, *J. Chem. Phys.*, 2008, **128**, 134501.
34 J.-F. Côté, D. Brouillette, J. E. Desnoyers, J.-F. Rouleau, J.-M. St-Arnaud and G. Perron, *J. Solution Chem.*, 1996, **25**, 1163–1173.
35 C. Daguenet, P. J. Dyson, I. Krossing, A. Oleinikova, J. Slattery, C. Wakai and H. Weingärtner, *J. Phys. Chem. B*, 2006, **110**, 12682–12688.
36 M. Sega and C. Schröder, *J. Phys. Chem. A*, 2015, **119**, 1539–1547.
37 A. Peyman, C. Gabriel and E. H. Grant, *Bioelectromagnetics*, 2007, **28**, 264–274.
38 R. M. Adar, S. A. Safran, H. Diamant and D. Andelman, *Phys. Rev. E: Stat., Nonlinear, Soft Matter Phys.*, 2019, **100**, 042615.
39 N. Gavish, D. Elad and A. Yochelis, *J. Phys. Chem. Lett.*, 2018, **9**, 36–42.
40 B. Rotenberg, O. Bernard and J.-P. Hansen, *J. Phys.: Condens. Matter*, 2018, **30**, 054005.
41 R. Kjellander, *Soft Matter*, 2019, **15**, 5866–5895.
42 M. Han and R. M. Espinosa-Marzal, *J. Phys. Chem. C*, 2018, **122**, 21344–21355.
43 M. Han and R. M. Espinosa-Marzal, *ACS Appl. Mater. Interfaces*, 2019, **11**, 33465–33477.
44 N. Hjalmarsson, R. Atkin and M. W. Rutland, *Chem. Commun.*, 2017, **53**, 647–650.